JOURNAL OF CHEMICAL & ENGINEERING DATA

ARTICLE

pubs.acs.org/jced

Vapor-Phase Mole Fractions Determined from the *P*, *x* Data Using the Margules Equation for High-Pressure Binary Vapor−Liquid Equilibrium Systems Including Carbon Dioxide

Satoru Kato,*[,†] Juergen P. Schmelzer,[‡] Peter Gostomski,[§] and Kenneth N. Marsh[§]

[†]Department of Applied Chemistry, Tokyo Metropolitan University, Minamiohsawa, Hachiohji, 192-0397, Japan

[‡]Department of Chemical Engineering, University of Applied Sciences, Friedrich-List-Platz 1, 01069 Dresden, Germany

[§]Department of Chemical and Process Engineering, University of Canterbury, Christchurch 8140, New Zealand

ABSTRACT: High-pressure *P*, *x* data for CO_2 + hydrocarbons, methanol, ethanol, and water binaries were correlated using the Margules equation. The average relative difference between experimental data and the correlation was as low as 1 % at $T < T_{c1}$, where T and T_{c1} denote the system temperature and the critical temperature of the lighter component. It was found that the average relative difference of the vapor phase mole fractions from the Margules equation representing the *P*, *x* data is 0.6 % for the asymmetric and nonazeotropic binaries. A criterion for identifying the nonazeotropic binaries is proposed. The strength of molecular interactions and molecular order were identified for the azeotropic and zeotropic mixtures using partial molar excess enthalpies and entropies at infinite dilution. A method for the high-precision correlation of infinite dilution activity coefficients is proposed.

INTRODUCTION

High pressure binary vapor−liquid equilibria (VLE) for mixtures of carbon dioxide and light hydrocarbons are of practical importance for the optimum design of natural gas treatment processes.[1] Further, high-pressure VLE data for mixtures of CO_2 and alkanols, such as methanol and ethanol, are required for the process development of industrial immobilization for CO_2 byproducts.[2] In addition, VLE data for mixtures of CO_2 and water have become important for the rational design not only of industrial CO_2 immobilization[2] but also for biological carbon capture.[3] Equations of state (EoS) combined with mixing rules have been known to satisfactorily correlate the high-pressure *P*, *x* data, as well as *P*, *y* data, for the mixtures including CO_2.[4−9] However, investigations predicting thermodynamic properties including partial molar quantities at high pressures are rare. It was recently shown[10] that high-pressure *P*, *x* data can be correlated simply using the Margules equation for few binaries including CO_2. Unfortunately, this promising method has not been applied to the calculation of *P*, *y* data and partial molar excess quantities that reflect the strength of molecular interactions and molecular order. Even for low-pressure VLE, the *P*, *y* data for azeotropic mixtures are not accurate.[11] Therefore, it is important for the practical treatment of high-pressure VLE data to determine if, for high-pressure nonazeotropic binaries, the *P*, *y* relationships are accurately calculated using the Margules equation derived from the *P*, *x* data. In addition, an advantage of the method using the Margules equation allows us to analyze the strength of the molecular interactions and molecular order even at high pressures.

The purpose of the present investigation is to show the following: (i) all of the high-pressure *P*, *x* data can be satisfactorily correlated using the Margules equation for the CO_2 + light hydrocarbons, methanol, ethanol, and water binaries; (ii) the Margules equation satisfactorily derives the *P*, *y* relationships of the nonazeotropic binaries identified by a criterion proposed in the present investigation; and (iii) the strength of molecular interactions and molecular order for the azeotropic and zeotropic mixtures are identified using the partial molar excess enthalpies and entropies. To eliminate the obscurity arising from the definition of hypothetical liquids,[10,12] constant temperature VLE data satisfying $T < T_{c1}$ are used, where T and T_{c1} denote the system temperature and the critical temperature of the lighter component. The present investigation proposes a practical calculation method for *P*, *y* relationships, because, in general, they involve higher experimental uncertainties than the *P*, *x* data.[4]

MODELS

Lumped Nonideality (LNI) Correlation. Binary vapor−liquid equilibria at constant temperature, T, are formulated as follows:[13]

$$Py_i = \Phi_i x_i P_{is} \quad (i = 1, 2) \tag{1}$$

$$\Phi_i = \gamma_i^{(P_a)} \frac{\phi_{is}}{\phi_i^{V}} \exp \frac{\overline{V}_i^{L}(P - P_a)}{RT} \exp \frac{V_i^{o}(P - P_{is})}{RT} \tag{2}$$

where x_i and y_i respectively denote the mole fractions of component i in the liquid phase and in the vapor phase. Equation 1 relates y_i to x_i. In eq 1, P and P_{is} are the system pressure and the vapor pressure of pure component i, respectively, while ϕ_i^{V} denotes the vapor phase fugacity coefficient of component i in the mixture at P and ϕ_{is} is the fugacity coefficient of the saturated vapor i at P_{is}. Furthermore, $\overline{V}_i^{L}$, V_i^{o}, and $\gamma_i^{(P_a)}$ respectively denote the partial molar volume of component i, the molar volume of

Special Issue: Kenneth N. Marsh Festschrift

Received: July 31, 2011
Accepted: October 31, 2011
Published: November 15, 2011

Table 1. VLE Parameters and Data Sources for the CO_2 + Hydrocarbons, Water, Methanol, and Ethanol Binaries

system	T/K	T/T_{c1}	P_{1s}/MPa	P_{2s}/MPa	n^a	$x_{1min}{}^b$	$x_{1max}{}^{b,c}$	A	B	$(ARD)_P{}^d$	$(ARD)_y{}^e$	X^f	Y^g	ref
Symmetric and Azeotropic Mixtures														
CO_2 (1) + ethane (2)	260.00	0.85	2.42	1.72	13	0	1	0.905	1.300	0.0071	0.1683	0.455	−0.685	15
CO_2 (1) + ethane (2)	283.15	0.93	4.51	3.03	14	0	0.80	0.327	1.323	0.0122		0.724	−1.576	16
CO_2 (1) + ethane (2)	269.25	0.89	3.14	2.18	15	0	1	0.674	1.283	0.0040		0.557	−0.906	16
CO_2 (1) + ethane (2)	255.34	0.84	2.11	1.52	17	0	1	0.906	1.328	0.0053		0.408	−0.616	16
CO_2 (1) + ethane (2)	241.45	0.79	1.35	1.01	11	0	1	0.984	1.447	0.0037		0.282	−0.465	16
CO_2 (1) + ethane (2)	252.95	0.83	1.96	1.42	15	0	1	0.964	1.319	0.0032	0.0860	0.384	−0.561	17
CO_2 (1) + ethane (2)	288.71	0.95	5.17	3.43	7	0.22	0.85	0.298	1.351	0.0109	0.2089	0.795	−2.042	18
CO_2 (1) + ethane (2)	266.48	0.88	2.91	2.03	12	0.07	0.92	0.703	1.297	0.0121	0.1979	0.525	−0.845	18
CO_2 (1) + ethane (2)	244.26	0.80	1.49	1.10	9	0.17	0.91	0.946	1.489	0.0098	0.0816	0.305	−0.543	18
CO_2 (1) + ethane (2)	222.04	0.73	0.65	0.53	12	0.13	0.88	1.206	1.782	0.0054	0.0451	0.150	−0.366	18
CO_2 (1) + ethane (2)	293.15	0.96	5.74	3.78	10	0	1	0.436	1.148	0.0074	0.2310	0.853	−1.709	19
CO_2 (1) + ethane (2)	283.15	0.93	4.51	3.03	15	0	1	0.531	1.219	0.0069	0.1403	0.724	−1.318	19
CO_2 (1) + ethane (2)	263.15	0.87	2.65	1.87	13	0	1	0.730	1.319	0.0040	0.0881	0.489	−0.784	19
CO_2 (1) + ethane (2)	243.15	0.80	1.43	1.07	14	0	1	0.938	1.458	0.0048	0.0541	0.296	−0.500	19
CO_2 (1) + ethane (2)	223.15	0.73	0.68	0.55	13	0	1	1.203	1.658	0.0046	0.0368	0.156	−0.325	19
CO_2 (1) + ethane (2)	250.00	0.82	1.79	1.31	15	0	1	0.856	1.435	0.0044	0.0815	0.356	−0.608	19
CO_2 (1) + ethane (2)	298.15	0.98	6.45	4.20	8	0	1	0.447	1.045	0.0037	0.3189	0.919	−1.726	20
CO_2 (1) + ethane (2)	293.15	0.96	5.74	3.78	13	0	1	0.511	1.14	0.0077	0.2652	0.853	−1.682	20
CO_2 (1) + ethane (2)	291.15	0.96	5.48	3.62	18	0	1	0.508	1.213	0.0089	0.1932	0.827	−1.777	20
CO_2 (1) + ethane (2)	288.15	0.95	5.10	3.39	17	0	1	0.514	1.253	0.0042	0.1746	0.788	−1.692	20
CO_2 (1) + ethane (2)	283.15	0.93	4.51	3.03	18	0	1	0.589	1.225	0.0022	0.1567	0.724	−1.332	20
CO_2 (1)−ethylene (2)	263.15	0.93	2.65	3.24	13	0	1	0.495	0.531	0.0022	0.0443	0.555	−0.692	21
CO_2 (1)−ethylene (2)	243.15	0.86	1.43	1.94	11	0	1	0.481	0.645	0.0066	0.0297	0.362	−0.417	21
CO_2 (1)−ethylene (2)	223.15	0.79	0.68	1.07	13	0	1	0.572	0.709	0.0040	0.0278	0.207	−0.234	21
CO_2 (1)−ethylene (2)	252.95	0.90	1.96	2.52	15	0	1	0.526	0.583	0.0027	0.0453	0.453	−0.524	21
CO_2 (1)−ethylene (2)	231.55	0.82	0.95	1.39	12	0	1	0.555	0.758	0.0031	0.0296	0.266	−0.336	21
Av.										0.0058	0.1230			
Zeotropic Mixtures														
CO_2 (1) + propane (2)	300.00	0.99	6.72	1.000	4	0.07	0.47	0.254	0.309	0.0078	0.2139	0.922	0.840	22
CO_2 (1) + propane (2)	303.15	1.00	7.22	1.081	16	0	1	0.183	0.222	0.0064	0.1726	0.981	0.932	6
CO_2 (1) + propane (2)	293.15	0.96	5.74	0.838	17	0	1	0.303	0.461	0.0043	0.1405	0.800	0.674	6
CO_2 (1) + propane (2)	283.15	0.93	4.51	0.638	16	0	1	0.437	0.633	0.0042	0.1170	0.642	0.491	6
CO_2 (1) + propane (2)	273.15	0.90	3.49	0.476	17	0	1	0.505	0.828	0.0052	0.0868	0.505	0.348	6
CO_2 (1) + propane (2)	263.15	0.87	2.65	0.346	16	0	1	0.635	1.008	0.0071	0.0702	0.388	0.242	6
CO_2 (1) + propane (2)	253.15	0.83	1.97	0.245	16	0	1	0.747	1.171	0.0070	0.0526	0.291	0.166	6
CO_2 (1) + propane (2)	273.15	0.90	3.49	0.476	12	0	1	0.787	1.002	0.0141	0.0895	0.505	0.318	21
CO_2 (1) + propane (2)	252.95	0.83	1.96	0.243	12	0	1	0.612	1.085	0.0163	0.0313	0.289	0.174	21
CO_2 (1) + propane (2)	266.48	0.88	2.91	0.386	11	0.09	0.82	0.524	0.973	0.0215	0.0624	0.425	0.271	23
CO_2 (1) + propane (2)	244.26	0.80	1.49	0.176	10	0.11	0.81	0.790	1.295	0.0094	0.0337	0.220	0.117	23
CO_2 (1) + propane (2)	294.26	0.97	5.89	0.863	17	0	1	0.310	0.398	0.0032	0.1135	0.819	0.707	24
CO_2 (1) + propane (2)	277.59	0.91	3.92	0.544	12	0	1	0.489	0.654	0.0062	0.0740	0.563	0.420	24
Av.										0.0087	0.0970			
Asymmetric and Nonazeotropic Binaries														
CO_2 (1)−hexane (2)	298.15	0.98	6.45	0.020	10	0.05	0.89	0.318	0.204	0.0305	0.0122	0.874	0.872	25
CO_2 (1)−benzene (2)	298.15	0.98	6.45	0.013	7	0.20	0.91	0.311	0.425	0.0216	0.0054	0.874	0.872	25
CO_2 (1)−pentane (2)	277.65	0.91	3.93	0.030	12	0	1	0.575	0.634	0.0152	0.0093	0.534	0.526	26
CO_2 (1)−methanol (2)	303.15	1.00	7.22	0.022	7	0.08	0.47	0.796	1.775	0.0104	0.0078	0.979	0.964	27
CO_2 (1)−methanol (2)	298.15	0.98	6.45	0.017	6	0.10	0.54	0.642	1.894	0.0207	0.0077	0.874	0.860	27
CO_2 (1)−methanol (2)	298.15	0.98	6.45	0.017	31	0.03	1	0.784	1.900	0.0236	0.0040	0.874	0.860	28
CO_2 (1)−methanol (2)	293.15	0.96	5.74	0.013	7	0.06	1	0.819	1.848	0.0150	0.0006	0.778	0.768	28
CO_2 (1)−methanol (2)	290.00	0.95	5.33	0.011	9	0.06	0.97	0.764	1.935	0.0253	0.0023	0.722	0.713	29

dx.doi.org/10.1021/je200842c |J. Chem. Eng. Data 2011, 56, 4927–4934

Table 1. Continued

system	T/K	T/T_{c1}	P_{1s}/MPa	P_{2s}/MPa	n^a	$x_{1min}{}^b$	$x_{1max}{}^{b,c}$	A	B	$(ARD)_P{}^d$	$(ARD)_y{}^e$	X^f	Y^g	ref
CO_2 (1)−methanol (2)	303.18	1.00	7.23	0.022	16	0.07	0.88	0.522	1.663	0.0181	0.0080	0.979	0.966	30
CO_2 (1)−methanol (2)	298.16	0.98	6.45	0.017	17	0.07	0.88	0.593	1.645	0.0199	0.0075	0.874	0.864	30
CO_2 (1)−methanol (2)	291.15	0.96	5.48	0.012	12	0.06	0.88	0.542	1.026	0.0128	0.0063	0.742	0.739	30
CO_2 (1)−methanol (2)	298.15	0.98	6.45	0.017	8	0.06	0.90	0.620	1.663	0.0269	0.0044	0.874	0.863	25
CO_2 (1)−methanol (2)	298.15	0.98	6.45	0.017	9	0.10	0.88	0.671	2.189	0.0166	0.0040	0.874	0.855	31
CO_2 (1)−methanol (2)	288.15	0.95	5.10	0.010	7	0.11	0.84	0.841	2.355	0.0355	0.0014	0.691	0.677	31
CO_2 (1)−ethanol (2)	303.15	1.00	7.22	0.010	9	0.06	0.91	0.694	1.701	0.0173	0.0041	0.979	0.972	32
CO_2 (1)−ethanol (2)	293.15	0.96	5.74	0.006	8	0.05	0.81	0.804	1.855	0.0257	0.0014	0.778	0.773	32
CO_2 (1)−ethanol (2)	298.00	0.98	6.42	0.008	9	0.01	0.03	0.850	2.473	0.0176	0.0000	0.870	0.859	33
CO_2 (1)−ethanol (2)	303.13	1.00	7.22	0.010	11	0.10	0.85	0.432	1.214	0.0292	0.0097	0.978	0.975	30
CO_2 (1)−ethanol (2)	298.17	0.98	6.45	0.008	8	0.13	0.81	0.104	1.089	0.0254	0.0093	0.874	0.871	30
CO_2 (1)−ethanol (2)	303.12	1.00	7.22	0.010	11	0.10	0.85	0.432	1.214	0.0292	0.0097	0.978	0.975	34
CO_2 (1)−ethanol (2)	298.17	0.98	6.45	0.008	8	0.13	0.81	0.104	1.089	0.0254	0.0093	0.874	0.871	34
Av.										0.0220	0.0059			
CO_2 (1)−water (2)	298.28	0.98	6.46	0.003	7	0.003	0.023	3.10	16.4	0.0259		0.876	−5680	33
CO_2 (1)−water (2)	288.26	0.95	5.11	0.002	7	0.004	0.028	3.07	14.8	0.0255		0.692	−638.0	33
CO_2 (1)−water (2)	278.22	0.91	3.98	0.001	6	0.006	0.020	3.00	11.8	0.0063		0.540	−14.8	35
CO_2 (1)−water (2)	293.00	0.96	5.72	0.002	9	0.001	0.002	3.21	11.7	0.0113		0.775	−35.9	35
CO_2 (1)−water (2)	288.00	0.95	5.08	0.002	14	0.001	0.004	3.15	15.9	0.0165		0.688	−1800	35
Av.										0.0171				

[a] Number of the data points. [b] Minimum x_1 value. [c] Maximum x_1 value. [d] Optimized average relative deviation, $(1/n)\Sigma|(P_{i,exp} - P_{i,cal})/P_{i,exp}|$. [e] Deviation in y_1, $(1/n)\Sigma|(y_{i,exp} - y_{i,cal})/y_{i,exp}|$, where $y_{i,cal}$ was calculated from the Margules equation. [f] $(P_{1s} + P_{2s})/(P_{c1} + P_{2s})$. [g] $(P_{1s} - P_{2s}e^B)/(P_{c1} - P_{2s})$.

pure liquid i at T, and the activity coefficient of the component i in the liquid phase at $P = P_a$, a reference pressure. Hereafter, the P_a value is fixed at 0 for simplicity, and $\gamma_i^{(P_a)}$ is abbreviated as γ_i. The standard state for the activity of component i is the pure liquid of i at T and P_a. The lumped nonideality (LNI) correlation uses the Margules equation for formulating Φ_1 and Φ_2 as follows:[10]

$$\ln \Phi_1 = {x_2}^2[A + 2(B - A)x_1] \tag{3}$$

$$\ln \Phi_2 = {x_1}^2[B + 2(A - B)x_2] \tag{4}$$

$$A = \ln {\Phi_1}^\infty \qquad B = \ln {\Phi_2}^\infty \tag{5}$$

where A and B denote the binary parameters. In the LNI correlation, the DECHEMA Chemistry Data Series analyzed low-pressure VLE data using the LNI correlation.[11] Meanwhile, Kato[10] applied the LNI correlation to the high-pressure P, x data including the $N_2 + O_2$, CO_2 + ethane, CO_2 + decane, and CO_2 + methanol binaries. In the latter section, all of the binaries including CO_2 are correlated using the following optimization for the average relative deviation, $(ARD)_P$

$$(ARD)_P = \frac{1}{n}\sum_{i=1}^{n}\left|\frac{P_{i,exp} - P_{i,cal}}{P_{i,exp}}\right| \tag{6}$$

where n denotes the number of the data points involved in one data set. The ratio of the fugacity coefficients of pure saturated vapors 1 and 2, ϕ_{1s}/ϕ_{2s}, is close to unity for the symmetric CO_2 + ethane and CO_2 + ethylene binaries. Therefore, in the latter section, it is shown that the LNI correlation satisfactorily represents the high-pressure P, x data for these symmetric systems. Furthermore, it is shown that the average deviation from the LNI correlation using 216 binaries including asymmetric systems is merely 0.9 %. An important advantage of the LNI correlation is that P, x data can be simply correlated using the constant parameters, A and B, which are independent of composition and pressure, although the expression of nonideality is complicated as shown in eq 2. In the latter section, a high-precision correlation of temperature effects on the A and B parameters is proposed.

A Criterion Identifying Asymmetric and Nonazeotropic Binaries. Fixing the lighter component as component 1, minimum azeotropic mixtures may be characterized as follows:

$$\left.\frac{dP}{dx_1}\right|_{x_1=1} < 0 \quad \text{at} \quad T < T_{c1} \tag{7}$$

Using the Margules equation, the left-hand side of eq 7 is identical with $P_{1s} - P_{2s}e^B$. Therefore, in the present investigation, the following nondimensional formula is tested for categorizing the nonazeotropic binaries:

$$\frac{P_{1s} - P_{2s}e^B}{P_{c1} - P_{2s}} = \frac{P_{1s} + P_{2s}}{P_{c1} + P_{2s}} \tag{8}$$

At $T \to 0$ and $P \to 0$, both $X = (P_{1s} + P_{2s})/(P_{c1} + P_{2s})$ and $Y = (P_{1s} - P_{2s}e^B)/(P_{c1} - P_{2s})$ approach zero. One of the advantages of using X and Y is that $X = Y$ $(= P_{1s}/P_{1c})$, eq 8, holds for the asymmetric binaries satisfying $P_{1s} \gg P_{2s}$. Furthermore, X is an index of proximity ratio to critical points, because $X < 0.1$ and $X > 0.1$, respectively, hold for the low- and high-pressure VLE data. Finally, $Y < 0$ holds for the azeotropic mixtures.

Partial Molar Excess Enthalpies and Entropies. Assuming ${\phi_i}^V = \phi_{is}$ and $\exp[(V_i^\circ(P - P_{is}))/RT] = 1$ for the symmetric systems, the activity coefficient in eq 2 is approximated at infinite dilution as follows:

$$\gamma_i^\infty = \frac{{\Phi_i}^\infty}{\exp({\bar{V}_i}^{L,\infty}p_{js}/RT)} \tag{9}$$

dx.doi.org/10.1021/je200842c |J. Chem. Eng. Data 2011, 56, 4927–4934

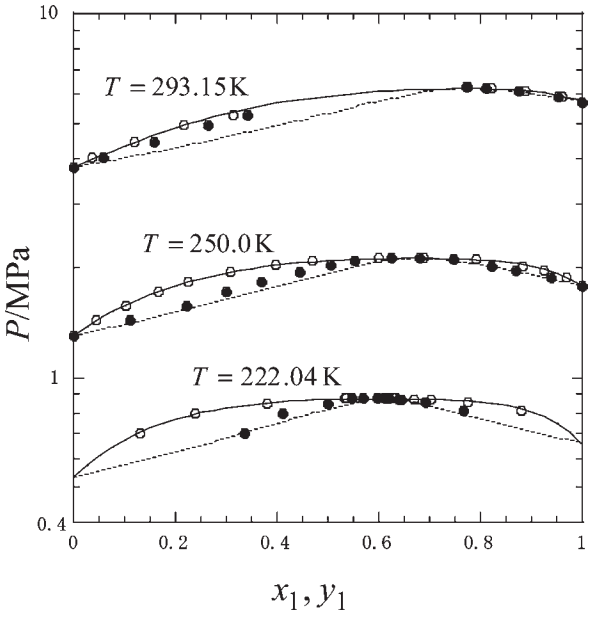

Figure 1. P vs x_1 and y_1 for the CO_2 (1) + ethane (2) binary at T = 222.04 K, 250.0 K, and 293.15 K: ○, P, x data; ●, P, y data; —, P, x relationships correlated using the Margules equation; - - -, P, y relationships calculated by the Margules equation representing the P, x data; data were cited from Fredenslund and Mollerup[18] at T = 222.04 K and Davalos et al. at T = 250.0 K and 293.15 K.[19]

where R denotes the gas constant. In the latter section, $\overline{V}_i^{L,\infty}$ was calculated using the nondimensional correlation proposed by Lyckman et al.[14] The partial molar excess enthalpy and entropy at infinite dilution of the component i, $H_i^{E,\infty}$ and $S_i^{E,\infty}$, respectively, are defined as follows:

$$\ln \gamma_i^{\infty} = \frac{H_i^{E,\infty}}{RT_o}\frac{T_o}{T} - \frac{S_i^{E,\infty}}{R} \quad (10)$$

where T_0 = 298.15 K is used. In the latter section, assuming $\phi_i^V = \phi_{is}$ and $\exp[(V_i^o(P - P_{is}))/RT] = 1$ for the symmetric systems, the $H_i^{E,\infty}/RT_0$ and $S_i^{E,\infty}/R$ values are calculated from the $A = \ln \Phi_1^{\infty}$ and $B = \ln \Phi_2^{\infty}$ values representing the P, x data.

Data Sources. Table 1 lists the data sources[15−35] used for the analysis. Six binaries, CO_2 (1) + ethane (2), CO_2 (1) + ethylene (2), CO_2 (1) + propane (2), CO_2 (1) + methanol (2), CO_2 (1) + ethanol (2), and CO_2 (1) + water (2), were extensively examined. The Wagner equation was used for calculating the vapor pressures of pure substances.[4]

RESULTS AND DISCUSSION

LNI Correlation. The Margules equation was fitted to the P, x data using the Marquardt method for determining the A and B parameters. The A and B values and the optimum $(ARD)_P$ values are listed in Table 1. The average relative differences were 0.6 %, 0.4 %, and 0.9 % for CO_2 (1) + ethane (2), CO_2 (1) + ethylene (2), and CO_2 (1) + propane (2), respectively. The average $(ARD)_P$ value of the six binaries is as low as 1.3 %, which is lower than the 1.8 % obtained from the 60 low-pressure VLE data sets of the methanol (1) + water (2) binary.[11] In Figure 1, P is plotted versus x_1 for the CO_2 (1) + ethane (2) binary at 222.04 K, 250.0 K, and 293.15 K. Figure 1 shows that the agreement between the experimental P, x data and their LNI correlations is excellent.

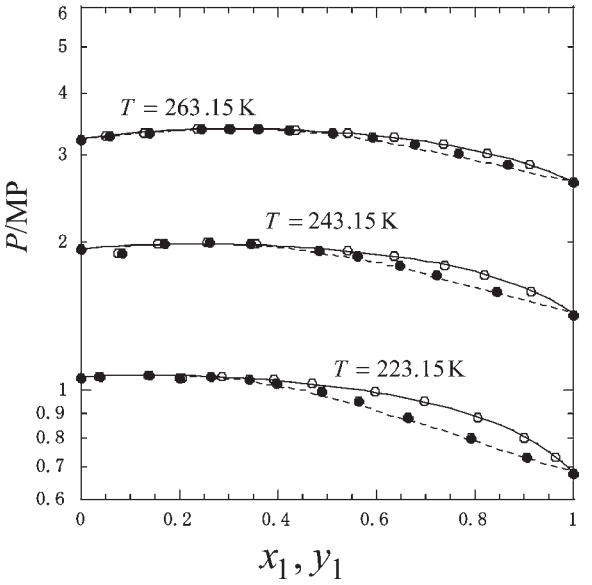

Figure 2. P vs x_1 and y_1 for the CO_2 (1) + ethylene (2) binary at T = 223.15 K, 243.15 K, and 263.15 K: ○, P, x data; ●, P, y data; —, P, x relationships correlated using the Margules equation; - - -, P, y relationships calculated by the Margules equation representing the P, x data; data were cited from Nagahama et al.[21]

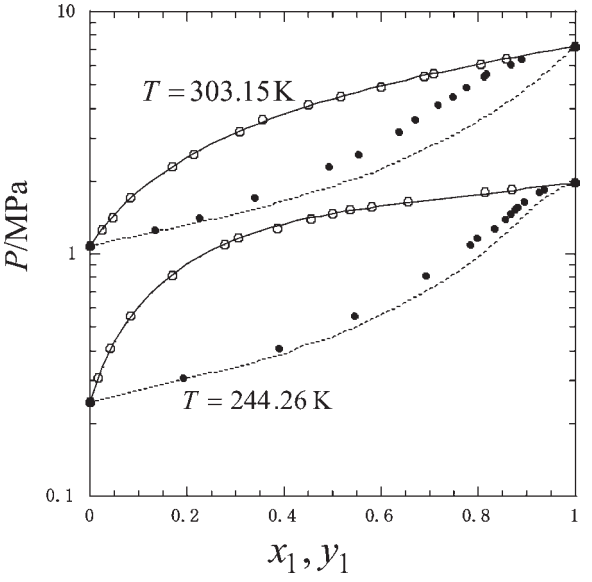

Figure 3. P vs x_1 and y_1 for the CO_2 (1) + propane (2) binary at T = 244.26 K and 303.15 K: ○, P, x data; ●, P, y data; —, P−x relationships correlated using the Margules equation; - - -, P, y relationships calculated by the Margules equation representing the P, x data; data were cited from Hamam and Lu at T = 244.26 K[23] and Kim and Kim at T = 303.15 K.[6]

In Figures 2 to 5, P is plotted versus x_1 for the CO_2 (1) + ethylene (2), CO_2 (1) + propane (2), CO_2 (1) + pentane (2), and CO_2 (1) + methanol (2) binaries. Figures 1 to 5 show that the P, x data can be satisfactorily correlated by the Margules equation. Equations of state (EoS) also satisfactorily correlate the P, x data. If the P, x data for CO_2 (1) + propane (2) at 253.15 K < T < 303.15 K reported by Kim and Kim[6] are used, the average relative differences from the Peng−Robinson equation of state (PR EoS) using interaction parameters involved in the mixing rules are as

dx.doi.org/10.1021/je200842c |J. Chem. Eng. Data 2011, 56, 4927–4934

Table 2. Correlation Deviations for the High- and Low-Pressure Binary *P*, *x* Data

	av.	asymmetric[a]	symmetric[b]	azeotropic
High-Pressure VLE Data[36,c]		$(ARD)_P$ (no. data sets)		
Margules	0.009(216)	0.020(18)	0.0076(198)	0.0069(37)
Wilson	0.012(216)	0.032(18)	0.011(198)	0.010(37)
NRTL[d]	0.018(216)	0.059(18)	0.014(198)	0.016(37)
Low-Pressure VLE Data[11]		$(ARD)_P$ from the Margules Equation (no. data sets)		
aqueous compounds	0.042(508)	-(0)	0.042(508)	0.048(268)
organic hydroxy compounds	0.027(1901)	0.024(64)	0.027(1837)	0.028(982)
aldehydes, ketones, ethers	0.012(1399)	0.010(92)	0.015(1307)	0.013(379)
carboxylic acids, anhydrides, esters	0.023(234)	0.016(5)	0.023(229)	0.031(57)
aliphatic hydrocarbons	0.012(1583)	0.018(108)	0.011(1475)	0.012(454)
aromatic hydrocarbons	0.010(1007)	0.024(60)	0.009(947)	0.007(108)
halogen, nitrogen, sulfur, and others	0.014(630)	0.016(59)	0.014(571)	0.015(134)

[a] Asymmetric mixtures satisfy $p_{2s}/p_{1s} < 0.01$. [b] Symmetric mixtures satisfy $p_{2s}/p_{1s} > 0.01$. [c] Alkane + alkane binaries and binaries including CO_2 were eliminated. [d] Having a nonrandomness parameter of 0.3.

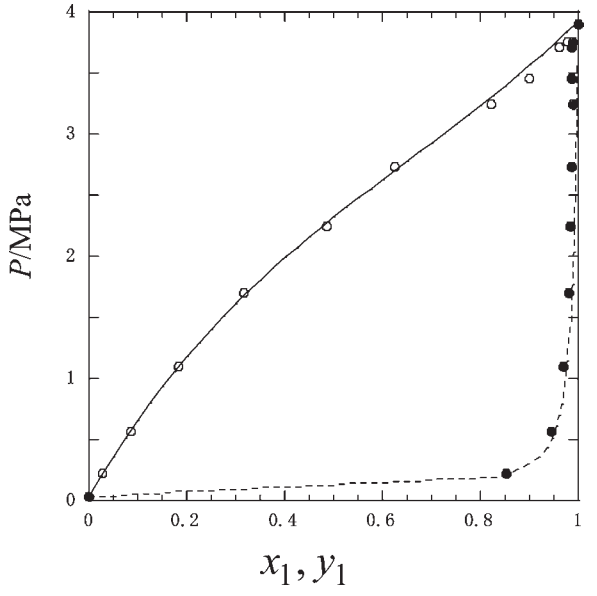

Figure 4. *P* vs x_1 and y_1 for the CO_2 (1) + pentane (2) binary at $T = 277.65$ K: ○, *P*, *x* data; ●, *P*, *y* data; —, *P*, *x* relationships correlated using the Margules equation; - - -, *P*, *y* relationships calculated by the Margules equation representing the *P*, *x* data; data were cited from Besserer and Robinson.[26]

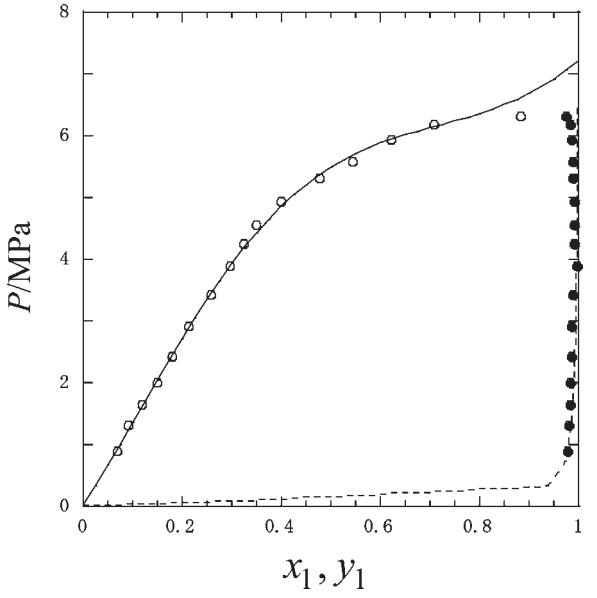

Figure 5. *P* vs x_1 and y_1 for the CO_2 (1) + methanol (2) binary at $T = 303.18$ K: ○, *P*, *x* data; ●, *P*, *y* data; —, *P*, *x* relationships correlated using the Margules equation; - - -, *P*, *y* relationships calculated by the Margules equation representing the *P*, *x* data; data were cited from Chang et al.[30]

low as 1.1 %[22] and 1.1 %.[6] The same value, 1.1 %, was reported using perturbed chain polar statistical associating fluid theory (PCP-SAFT).[8] Fortunately, the average $(ARD)_P$ value for the same data at 253.15 K < T < 303.15 K is almost half, that is, 0.6 %, demonstrating that the LNI correlation using the Margules equation is simple but satisfactorily represents the *P*, *x* data albeit using two binary parameters rather than one interaction parameter. If the nonrandom two-liquid (NRTL) equation with a nonrandomness parameter of 0.3 and Wilson equations are used instead of the Margules equation, the average $(ARD)_P$ values for the CO_2 (1) + propane (2) binary listed in Table 1 were 1 % and 0.9 %, respectively; that is, the Margules eq (0.9 %) provides an almost similar correlation.

As shown in Figures 1 to 3, the CO_2 (1) + ethane (2) and CO_2 (1) + ethylene (2) binaries form azeotropic mixtures, while the CO_2 (1) + propane (2) binary forms zeotropic mixtures. It is known that these symmetric systems show critical points at $T < T_{c1}$.[5] However, as shown in Figure 5, even asymmetric and nonazeotropic binaries show the same trend; that is, critical points appear at $T < T_{c1}$. This occurs throughout the nonazeotropic binaries including CO_2 (1) + hexane (2), CO_2 (1) + benzene (2), CO_2 (1) + methanol (2), and CO_2 (1) + ethanol (2). This might be the main reason that the $(ARD)_P$ values of the nonazeotropic binaries are higher than those of the azeotropic binaries. Similar results were obtained from the *P*, *x* data correlation using EoS and mixing rules.[36] As shown in Table 1, the average $(ARD)_P$ value from the nonazeotropic binaries is still as low as 2.2 %. The value for the CO_2 (1) + water (2) binary is also as low as 1.7 % in spite of its narrow x_1 ranges covering $0 < x_1 < 0.03$.

In Table 2, the deviations from the LNI correlation for asymmetric and symmetric mixtures are listed for 216 high-pressure[36]

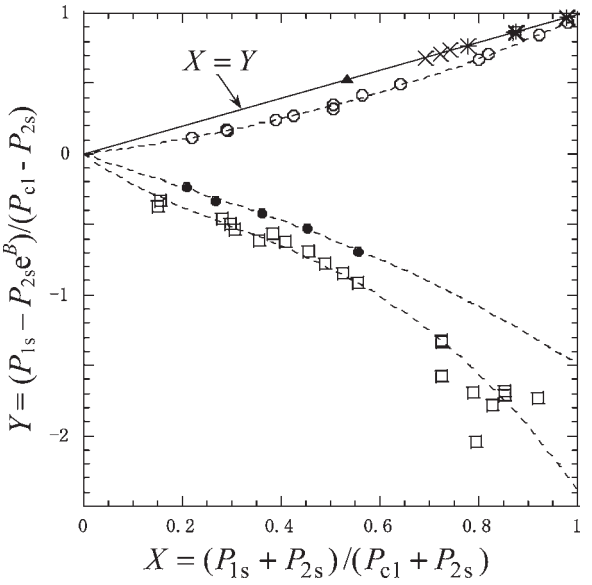

Figure 6. Y vs X: △, CO_2 (1) + hexane (2); ▽, CO_2 (1) + benzene (2); ▲, CO_2 (1) + pentane (2); ×, CO_2 (1) + methanol (2); +, CO_2 (1) + ethanol (2); ○, CO_2 (1) + propane (2); ●, CO_2 (1) + ethylene (2); □, CO_2 (1) + ethane (2); - - -, XY correlation.

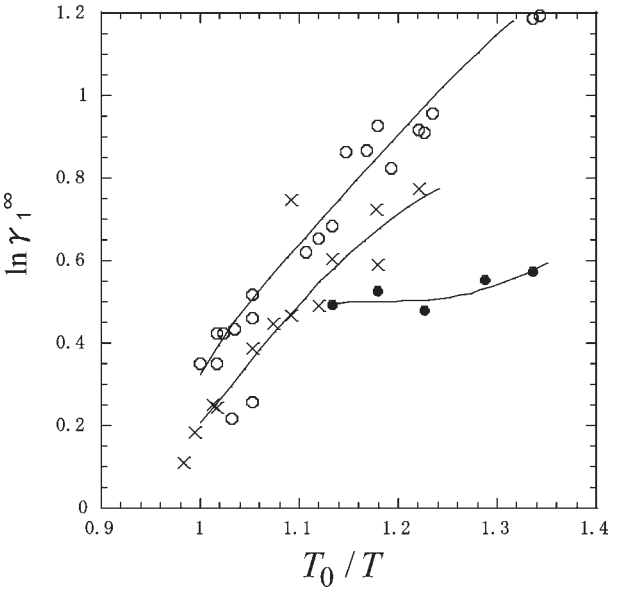

Figure 7. ln γ_1^∞ vs T_0/T: ○, CO_2 (1) + ethane(2); ●, CO_2 (1) + ethylene (2); ×, CO_2 (1) + propane (2); —, predicted using the high-precision XZ correlation; T_0 = 298.15 K.

and 7262 low-pressure[11] constant-temperature VLE data. Table 2 shows that the LNI correlation deviations from the Margules equation are notable for the low-pressure polar and symmetric binaries, which arises from azeotropic mixtures. Further, the correlation deviations of the high-pressure asymmetric binaries are as low as 2 % and almost identical with those of low-pressure asymmetric hydrocarbon binaries. Five of the 18 high-pressure asymmetric binaries satisfying $(ARD)_P > 2$ % show notable data scatter, while the other four include alkanols, and they show the critical point deviations at $T < T_{c1}$. Therefore, these low quality high-pressure data may have caused the notable LNI correlation deviations. As shown in Table 2, the LNI characteristics of high-pressure binaries are similar to those of low-pressure nonpolar binaries; therefore, the Margules equation provides a better correlation than the Wilson and NRTL equations. In summary, Tables 1 and 2 show that the LNI correlation satisfactorily represents the P, x data of the high-pressure binaries covering $T < T_{c1}$.

y_1 Predicted from the P, x Data and the Criterion for Nonazeotropic Binaries. Using the Margules equation, average relative deviations from the P, y data were evaluated as follows:

$$(ARD)_y = \frac{1}{n}\sum_{i=1}^{n}\left|\frac{y_{1i,\mathrm{exp}} - y_{1i,\mathrm{cal}}}{y_{1i,\mathrm{exp}}}\right| \qquad (11)$$

where $y_{1i,cal}$ was calculated by eqs 1, 3, and 4 with the A and B values representing the P, x data. Table 1 lists the $(ARD)_y$ values. Figures 1 to 5 include the calculated P, y relationships as dashed lines. In low-pressure VLE, it is known that the P, y data of azeotropic binaries are less satisfactorily predicted from the P, x data. Figures 1 to 3 show that the agreement between experimental and predicted P, y relationships is worse at high pressures approaching the critical points. However, Figures 4 and 5 show that they are excellent for the nonazeotropic binaries. In reality, as shown in Table 1, the average $(ARD)_y$ value of the nonazeotropic binaries approaches 0.6 %, which is much less than their average $(ARD)_P$ value, 2.2 %. Therefore, to demonstrate the simple and practical method for the P, y relationships, the criterion for the nonazeotropic binary, eq 8, should be examined. In Figure 6, $Y = (P_{1s} - P_{2s}e^B)/(P_{c1} - P_{2s})$ is plotted versus $X = (P_{1s} + P_{2s})/(P_{c1} + P_{2s})$. Figure 6 clearly shows that all of the nonazeotropic binaries meet the criterion of $X = Y$. The zeotropic mixture, CO_2 + propane, slightly deviates from the $X = Y$ relationship, while the azeotropic mixture, CO_2 + ethane, is located at $Y < 0$. Therefore, for the high-pressure VLE at $T < T_{c1}$, the P, y relationship is accurately calculated from accurate P, x data using the Margules equation, if eq 8 is satisfied. The application of eq 8 to low-pressure azeotropic mixtures should be examined in the future.

Partial Molar Excess Enthalpies and Entropies. To determine the strength of molecular interactions and molecular order, in Figure 7, ln γ_1^∞ is plotted versus T_0/T for the CO_2 (1) + ethane (2), CO_2 (1) + ethylene (2), and CO_2 (1) + propane (2) binaries. The γ_1^∞ values were calculated from eq 9 using an empirical nondimensional correlation.[13] Figure 7 shows that the scatter of infinite dilution activity coefficients is striking. Similar scatter appears in low-pressure data.[11] Without developing a high-precision correlation for the infinite dilution activity coefficients, it is impossible to determine accurate partial molar excess quantities. Fortuitously, the data convergence of the data appearing in Figure 6 suggests a high-precision correlation of the infinite dilution activity coefficients. Therefore, the high-precision correlation for γ_2^∞ is obtained using the following X and Y, which reflects nondimensional infinite dilution pressure slope at $x_1 = 1$:

$$X = \frac{P_{1s} + P_{2s}}{P_{c1} + P_{2s}} \qquad (12)$$

$$Y = \frac{P_{1s} - \gamma_2^\infty P_{2s}}{P_{c1} - P_{2s}} \qquad (13)$$

The high-precision correlation for γ_1^∞ is obtained using X and the following Z, which reflects the nondimensional infinite

Table 3. High-Precision Correlation of Infinite Dilution Activity Coefficients

system	correlation[a]	$(ARD)_Y$[b], $(ARD)_Z$[c]
CO_2 (1)−ethane (2)	$Z = -13.2947X + 4.3611X^2 + 15.3639\ln(1 + X)$	0.11
	$Y = 21.083X - 7.0916X^2 - 23.6339\ln(1 + X)$	0.07
CO_2 (1)−ethylene (2)	$Z = -12.6176X + 5.2356X^2 + 12.8192\ln(1 + X)$	0.09
	$Y = 3.5324X - 1.7118X^2 - 4.787\ln(1 + X)$	0.03
CO_2 (1)−propane (2)	$Z = -6.3643X + 1.4943X^2 + 8.7428\ln(1 + X)$	0.05
	$Y = -0.4542X + 0.7864X^2 + 0.911\ln(1 + X)$	0.02
CO_2 (1)−water (2)	$Z = 24.5053X^{1.2697}$	0.05

[a] $X = (P_{1s} + P_{2s})/(P_{c1} + P_{2s})$. [b] $(ARD)_Y = (1/n)\Sigma|(Y_{i,exp} - Y_{i,cal})/Y_{i,exp}|$. [c] $(ARD)_Z = (1/n)\Sigma|(Z_{i,exp} - Z_{i,cal})/Z_{i,exp}|$.

Table 4. $H_i^{E,\infty}/RT_0$ and $S_i^{E,\infty}/R$ Values for CO_2 + Ethane, Propane, Ethylene, and Water Binaries at 280 K[a]

system	$H_1^{E,\infty}/RT_0$	$S_1^{E,\infty}/R$	$H_2^{E,\infty}/RT_0$	$S_2^{E,\infty}/R$
CO_2 (1) + ethane(2)	2.8 (2.7)	2.3 (2.2)	1.3	0.09
CO_2 (1) + propane (2)	2.9 (2.6)	2.5 (2.2)	5.1	4.3
CO_2 (1) + ethylene (2)	2.1 (0.84)	1.7 (0.63)	3.8	3.4
CO_2 (1) + water (2)	−1.8 (−2.1)	−4.8 (−5.0)	−43	−59

[a] $T_0 = 298.15$ K.

dilution pressure slope at $x_1 = 0$:

$$Z = \frac{\gamma_1^{\infty} P_{1s} - P_{2s}}{P_{c1} - P_{2s}} \tag{14}$$

In Table 3, the correlation functions of the high-precision correlation are listed for four binaries. Table 3 shows that the correlation deviations are satisfactorily low. In Figure 6, the Y values calculated using XY correlations are plotted using dashed lines. Figure 6 shows that the lines are identical with the converged XY data reported by different authors using different equipment; that is, these lines represent accurate VLE relationships. Therefore, the high-precision XY and XZ correlations are practically useful for calculating not only VLE relationships but also data consistency. Furthermore, they are expected to theoretically promote the development of solution models.

In Figure 7, $\ln \gamma_1^{\infty}$ is plotted using solid lines. Figure 7 shows that the XZ correlation represents the scattering of γ_1^{∞} values. The partial molar excess quantities were calculated from eq 10 using the numerical differentiations of $\ln \gamma_i^{\infty}$ calculated from Y and Z in Table 3. In Table 4, the $H_i^{E,\infty}/RT_0$ and $S_i^{E,\infty}/R$ values at 280 K are listed. For convenience, hereafter, $H_{i,j}^{E,\infty}$ denotes the partial molar excess enthalpy of component i at infinite dilution in component j. Table 4 demonstrates that the molecular interactions of hydrogen bonding in water are much stronger than the interactions in hydrocarbons, because $H_{CO_2,hydrocarbon}^{E,\infty} \gg H_{CO_2,water}^{E,\infty}$ holds, which reflects strong interactions between a CO_2 molecule and the surrounding water molecules. Note that the interaction strength of a CO_2 molecule with ethane and propane molecules is almost the same but is weaker than that with ethylene molecules, because $H_{CO_2,ethane}^{E,\infty} = H_{CO_2,propane}^{E,\infty} > H_{CO_2,ethylene}^{E,\infty}$ holds. Both molecular interactions and molecular order have effects on $\ln \gamma_i^{\infty}$, because the $H_i^{E,\infty}/RT_0$ and $S_i^{E,\infty}/R$ values are almost the same in magnitude. In Table 4, the values in parentheses were calculated assuming $\overline{V}_i^{L,\infty} = 0$. The values in parentheses provide almost the same insight obtained from $\overline{V}_i^{L,\infty} \neq 0$. Table 4 includes the $H_2^{E,\infty}/RT_0$ and $S_2^{E,\infty}/R$ values of infinitely diluted solutes in CO_2. In this case, the standard states of activities are different in different solutes. However, Table 4 shows that propane in CO_2 exerts weak molecular interactions and molecular disorder, because the $H_{propane,CO_2}^{E,\infty}/RT_0$ and $S_{propane,CO_2}^{E,\infty}/R$ values are higher than those from ethane and ethylene. It is known that minimum azeotropic mixtures result from weak molecular interactions between solute and solvent molecules in the liquid phase.[37] Therefore, it might be that this weak molecular interaction originates the zeotropic behavior in spite of the nearly asymmetric CO_2 (1) + propane (2) binary. Table 4 includes the $H_{water,CO_2}^{E,\infty}/RT_0$ and $S_{water,CO_2}^{E,\infty}/R$ values, reflecting strong molecular interactions and high molecular order. Using infrared photodissociation spectra at 0.4 MPa, it has been identified that a water molecule is stabilized by the hydrogen bonding, OH−OCO, formed in the cluster involving seven CO_2 molecules;[38] therefore, the strong molecular interactions and high order may be ascribed to this hydrogen bonding in CO_2 clusters.

CONCLUSION

The correlation of high-pressure P, x data and the prediction of P, y relationships were investigated for the CO_2 + light hydrocarbons, methanol, ethanol, and water binaries, because they are important for the process development of natural gases, CO_2 immobilization, and biological carbon capture. It was shown that all of the P, x data can be satisfactorily correlated using the Margules equation. Furthermore, the Margules equation satisfactorily predicts the P, y relationships of the nonazeotropic binaries identified by the proposed criterion, eq 8. It was also shown that the slightly asymmetric and zeotropic CO_2 + propane binary has weaker molecular interactions and lower molecular order than the symmetric and azeotropic CO_2 + ethane binary. A method for the high-precision correlation of infinite dilution activity coefficients was proposed (readers can use the correlation at http://www.sskato.jp).

AUTHOR INFORMATION

Corresponding Author

*E-mail: kato-satoru@tmu.ac.jp.

Funding Sources

The authors are grateful to the University of Canterbury and Showa Denko K. K. for their support to the research collaboration.

ACKNOWLEDGMENT

The authors thank Shou Kurita for his devotion to literature collection for the CO_2 + alkanol binaries.

REFERENCES

(1) Rogers, W. J.; Bullin, J. A.; Davison, R. R.; Frazier, R. E.; Marsh, K. N. FTIR method for VLE measurements of acid-gas-alkanolamine systems. *AIChE J.* **1997**, *43*, 3223–3231.

(2) Tomishige, K.; Kunimori, K. Catalytic and direct synthesis of dimethyl carbonate starting from carbon dioxide using CeO_2-ZrO_2 solid solution heterogeneous catalyst: effect of H_2O removal from the reaction system. *Appl. Catal., A* **2002**, *237*, 103–109.

(3) Stucki, S.; Vogel, F.; Ludwig, C.; Hiduc, A. G.; Brandenberger, M. Catalytic gasification of algae in supercritical water for biofuel production and carbon capture. *Energy Environ. Sci.* **2009**, *2*, 535–541.

(4) Poling, B. E.; Prausnitz, J. M.; O'Connell, J. P. *The Properties of Gases and Liquids*; McGraw-Hill: New York, 2001.

(5) Horstmann, S.; Fischer, K.; Gmehling, J.; Kolar, P. Experimental determination of the critical line for (carbon dioxide + ethane) and calculation of various thermodynamic properties for (carbon dioxide + n-alkane) using the PSRK model. *J. Chem. Thermodyn.* **2000**, *32*, 451–464.

(6) Kim, J. H.; Kim, M. S. Vapor-liquid equilibria for the carbon dioxide + propane system over a temperature range from 253.15 to 323.15 K. *Fluid Phase Equilib.* **2005**, *238*, 13–19.

(7) Lopez, J. A.; Cardona, C. A. Phase equilibrium calculations for carbon dioxide + n-alkanes binary mixtures with the Wong-Sandler mixing rules. *Fluid Phase Equilib.* **2006**, *239*, 206–212.

(8) Tang, X.; Gross, J. Modeling the phase equilibria of hydrogen sulfide and carbon dioxide in mixture with hydrocarbons and water using the PCP-SAFT equation of state. *Fluid Phase Equilib.* **2010**, *293*, 11–21.

(9) Trejos, V. M.; Lopez, J. A.; Cardona, C. A. Thermodynamic consistency of experimental VLE data for asymmetric binary mixtures at high pressures. *Fluid Phase Equilib.* **2010**, *293*, 1–10.

(10) Kato, S. An empirical test using the thermodynamic consistency lines for the VLE data of 7262 constant-temperature and 5167 constant-pressure binaries. *Fluid Phase Equilib.* **2011**, *302*, 202–212.

(11) Gmehling, J.; Onken, U. Vapor-Liquid Equilibrium Data Collection. *DECHEMA Chemistry Data Series*, Vol. I, Parts 1 to 8a; DECHEMA: New York, 1977−2001.

(12) Kato, S. Prediction of Henry's constants for alkane/alkane binaries above solute critical. *AIChE J.* **2005**, *51*, 3275–3285.

(13) Prausnitz, J. M. *Molecular Thermodynamics of Fluid Phase Equilibria*; Prentice-Hall: Upper Saddle River, NJ, 1969.

(14) Lyckman, E. W.; Eckert, C. A.; Prausnitz, J. M. Generalized liquid volumes and solubility parameters for regular solution application. *Chem. Eng. Sci.* **1965**, *20*, 703–706.

(15) Clark, A. Q.; Stead, K. (Vapor + liquid) phase equilibria of binary, ternary, and quaternary mixtures of methane, ethane, propane, butane, and carbon dioxide. *J. Chem. Thermodyn.* **1988**, *20*, 413–428.

(16) Gugnoni, R. J.; Eldrige, J. W.; Okay, V. C.; Lee, T. J. Carbon dioxide-ethane phase equilibrium and densities from experimental measurements and the B-W-R equation. *AIChE J.* **1974**, *20*, 357–362.

(17) Hamam, S. E. M.; Lu, B. C. Y. Vapor-liquid equilibrium in the ethane-carbon dioxide system. *Can. J. Chem. Eng.* **1974**, *52*, 283–289.

(18) Fredenslund, A.; Mollerup, J. Measurement and prediction of equilibrium ratios for ethane + carbon dioxide system. *J. Chem. Soc., Faraday Trans. I* **1974**, *70*, 1653–1660.

(19) Davalos, J.; Anderson, W. R.; Phelps, R. E.; Kidnay, A. J. Liquid-vapor equilibria at 250.00 K for systems containing methane, ethane, and carbon dioxide. *J. Chem. Eng. Data* **1976**, *21*, 81–84.

(20) Ohgaki, K.; Katayama, T. Isothermal vapor-liquid equilibrium data for the ethane-carbon dioxide system at high pressures. *Fluid Phase Equilib.* **1977**, *1*, 27–32.

(21) Nagahama, K.; Konishi, H.; Hoshino, D.; Hirata, M. Binary vapor-liquid equilibriums of carbon dioxide-light hydrocarbons at low temperature. *J. Chem. Eng. Jpn.* **1974**, *7*, 323–329.

(22) Nagata, Y.; Mizutani, K.; Miyamoto, H. The precise measurement of the (vapor + liquid) equilibrium properties for (CO_2 + isobutene) binary mixtures. *J. Chem. Thermodyn.* **2011**, *43*, 244–247.

(23) Hamam, S. E. M.; Lu, B. C. Y. Isothermal vapor-liquid equilibriums in binary system propane-carbon dioxide. *J. Chem. Eng. Data* **1976**, *21*, 200–204.

(24) Reamer, H. H.; Sage, B. H.; Lacey, W. N. Phase equilibria in hydrocarbon systems. Volumetric and phase behavior of the propane-carbon dioxide system. *J. Ind. Eng. Chem.* **1951**, *43*, 2515–2520.

(25) Ohgaki, K.; Katayama, T. Isothermal vapor-liquid equilibrium data for binary systems containing carbon dioxide at high pressures: methanol-carbon dioxide, n-hexane-carbon dioxide, and benzene-carbon dioxide systems. *J. Chem. Eng. Data* **1976**, *21*, 53–55.

(26) Besserer, G. J.; Robinson, D. B. Equilibrium-phase properties of n-pentane-carbon dioxide system. *J. Chem. Eng. Data* **1973**, *18*, 416–419.

(27) Laursen, T.; Rasmussen, P.; Ivar, A. S. VLE and VLLE measurements of dimethyl ether containing systems. *J. Chem. Eng. Data* **2002**, *47*, 198–202.

(28) Secuianu, C.; Feroiu, V.; Geana, D. Phase equilibria experiments and calculations for carbon dioxide + methanol binary system. *Cent. Eur. J. Chem.* **2009**, *7*, 1–7.

(29) Hong, J. H.; Kobayashi, R. Vapor-liquid equilibrium studies for the carbon dioxide-methanol system. *Fluid Phase Equilib.* **1988**, *41*, 269–276.

(30) Chang, C. J.; Day, C.-Y.; Ko, C.-M.; Chiu, K.-L. Densities and *P-x-y* diagrams for carbon dioxide dissolution in methanol, ethanol, and acetone mixtures. *Fluid Phase Equilib.* **1997**, *131*, 243–258.

(31) Bezanehtak, K.; Combes, G. B.; Dehghani, F.; Foster, N. R. Vapor-liquid equilibrium for binary systems of carbon dioxide + methanol, hydrogen + methanol, and hydrogen + carbon dioxide at high pressures. *J. Chem. Eng. Data* **2002**, *47*, 161–168.

(32) Secuianu, C.; Feroiu, V.; Geana, D. Phase behavior for carbon dioxide + ethanol system. Experimental measurements and modeling with a cubic equation of state. *J. Supercrit. Fluids* **2008**, *47*, 109–116.

(33) Dalmolin, I.; Skovroinski, E.; Biasi, A.; Corazza, M. L.; Dariva, C.; Oliveira, J. V. Solubility of carbon dioxide in binary and ternary mixtures with ethanol and water. *Fluid Phase Equilib.* **2006**, *245*, 193–200.

(34) Day, C.-Y.; Chang, C. J.; Chen, C.-Y. Phase equilibrium of ethanol + CO_2 and acetone + CO_2 at elevated pressures (correction). *J. Chem. Eng. Data* **1999**, *44*, 365–365.

(35) Valtz, A.; Chapoy, A.; Coquelet, C.; Paricaud, P.; Richon, D. Vapor-liquid equilibria in the carbon dioxide-water system, measurement and modeling from 278.2 to 318.2 K. *Fluid Phase Equilib.* **2004**, *226*, 333–344.

(36) Knapp, H.; Doring, R.; Oellrich, L.; Plocker, U.; Prausnitz, J. M. Vapor-Liquid Equilibria for Mixtures of Low Boiling Substances. *DECHEMA Chemistry Data Series*, Vol. VI; DECHEMA: New York, 1982.

(37) Atkins, P. W. *Physical Chemistry*, 4th ed.; Oxford University Press: New York, 1990.

(38) Inokuchi, Y.; Kobayashi, Y.; Muraoka, A.; Nagata, T.; Ebata, Y. Structures of water-CO_2 and methanol-CO_2 cluster ions: $[H_2O\text{-}(CO_2)_n]^+$ and $[CH_3OH\text{-}(CO_2)_n]^+$ (n = 1−7). *J. Chem. Phys.* **2009**, *130*, 154304.